Fractals, Vol. 15, No. 4 (2007) 315–322

World Scientific
www.worldscientific.com

MATHEMATICAL IMAGING USING CHEMICAL REACTIONS DISCRETE CHAOTIC DYNAMICS

V. GONTAR* and O. GRECHKO
International Group for Chaos Studies
Department of Industrial Engineering and Management
Ben-Gurion University of the Negev
P.O. Box 653, Beer-Sheva 84105, Israel
**galita@bgu.ac.il*

Received January 16, 2007
Accepted May 5, 2007

Abstract

A specific system of difference equations derived from chemical reactions discrete chaotic dynamics (CRDCD) was used for generating visual images. Examples of symmetrical images generated by the proposed method were used to illustrate the impact of different color palettes on the resulting images. The image quality could be improved by applying an interpolation scheme.

Keywords: Mathematical Imaging; Discrete Chaotic Dynamics; Symmetrical Images.

1. INTRODUCTION

Mathematical imaging — a growing computer science domain — may be exploited in a variety of applications, such as visualization of physico-chemical processes, modeling of brain creativity, computer graphics and artwork. The different approaches used for mathematical imaging include fractals,[1,2] cellular automata,[3] L-systems[4] and evolutionary algorithms.[5]

Here we present an approach for mathematical imaging that exploits solutions of difference equations derived from the chemical reactions discrete chaotic dynamics (CRDCD).[6–9] When solved at a discrete time on a square lattice (discrete

space), these systems of difference equations generate sequences of 2D numerical arrays. Encoding of these 2D arrays in color (visualization) produces 2D images. It has been shown that by varying the parameters of the proposed difference equations, we can obtain a variety of images (patterns), including symmetrical images, spirals and rings.

In this paper, we thus analyze the impact of the visualization factors, such as type of color palette and nature of the interpolation scheme, on the resulting images. We show that visualization of discrete space-distributed concentrations with the different palettes provides a visual representation of the internal patterns that are embedded in the numerical source calculated with CRDCD (2D arrays of space-distributed concentrations of constituents). For improving the quality of the resulting images we use the interpolation of the calculated values of the constituents' concentrations. We also discuss ways of using the images generated with CRDCD to produce different animation effects. To demonstrate the proposed approach, we present and analyze the symmetrical images generated by the relevant CRDCD mathematical equations derived for a particular chemical transformation mechanism.

2. BACKGROUND

CRDCD basic equations are constructed according to the mechanism of transformation of chemical constituents (agents, A_i) expressed by a matrix of stoichiometric coefficients $\|\nu_{li}\|$. The equations formally take into consideration "information exchange" between the constituents [a special type of feedback between the constituents, denoted by black arrows in Eq. (1)]:

$$\sum_{i=1}^{N} \nu_{li} A_i \overset{\curvearrowright}{=} 0; \quad i = 1, 2, \ldots, N; \quad j = 1, 2, \ldots, M; \quad l = 1, 2, \ldots, N - M. \quad (1)$$

We consider the chemical reactions occurring on a discrete square lattice of final size $R \times R$, where each cell of the lattice is designated by integer coordinates $R_p, R_s = 1, 2, \ldots, R$ [p denotes rows (vertical direction) and s denotes columns (horizontal direction)]. According to CRDCD, any possible mechanism of transformation of constituents $(X_i, i = 1, 2, \ldots, N)$ represented by matrix $\|\nu_{li}\|$ can be mathematically modeled by the following system of nonlinear difference equations:

$$\prod_{i=1}^{N} (X_i^{t_q}(R_p, R_s))^{\nu_{li}} = \pi_l(t_{q-1}, r\otimes) \quad (2)$$

$$\pi_l(t_{q-1}, r\otimes) = k_l \exp\left\{ -\sum_{i=1}^{N} \alpha_{li} X_i^{t_{q-1}}(R_p, R_s) + \sum_{i=1}^{N} \beta_{li}^{r} X_i^{t_{q-1}}(r\otimes) \right\} \quad (3)$$

$$\sum_{i=1}^{N} a_{ij} X_i^{t_q}(R_p, R_s) = b_j \quad (4)$$

with the initial and boundary conditions:

$$X_i^{t_0}(R_p, R_s) = \begin{cases} b_j, & i = j \\ 0, & i = M+1, M+2, \ldots, N \end{cases} \quad (5)$$

$$X_i^{t_q}(R_p, R_s) = \begin{cases} X_i^{t_q}(R_p, R_s), & 1 \le R_p, R_s \le R \\ & \text{(inside the lattice)} \\ 0, & R_p, R_s < 1;\ R_p, R_s > R \\ & \text{(outside the lattice)} \end{cases} \quad (6)$$

where $X_i^{t_q}(R_p, R_s)$ is the concentration of the ith constituent that is calculated in each cell of the lattice with coordinates (R_p, R_s) and that characterizes the system's particular state at discrete time $t_q (q = 1, 2, \ldots, Q)$; $\|a_{ij}\|$ is a molecular matrix defining the number of components of type "j" in the ith constituent $(j = 1, 2, \ldots, M)$; $\pi_1(t_{q-1}, r\otimes)$ is a function of the concentrations of the system's constituents $X^{t_{q-1}}(R_p, R_s)$ calculated at a previous moment of discrete time t_{q-1} and of the neighboring concentrations $X_i^{t_{q-1}}(r\otimes)$; b_j is the total concentration of the jth main constituent; k_l is the rate constant for the lth reaction; α_{li} are empirical parameters that characterize the local "information exchange" taking place between the constituents inside the considered cell of the lattice; and β_{li}^{r} are empirical parameters that characterize the "information exchange" between the constituents in the eight closest neighboring cells, including the cell under consideration $(r = 1, 2, \ldots, 9)$, with coordinates denoted by: $r\otimes = [(R_p - 1, R_s - 1), (R_p - 1, R_s), (R_p - 1, R_s + 1), (R_p, R_s - 1), (R_p, R_s), (R_p, R_s + 1), (R_p + 1, R_s - 1), (R_p + 1, R_s), (R_p + 1, R_s + 1)]$.

To demonstrate the application of a CRDCD mathematical model for generating images, we use

the following mechanism describing the interaction between three chemical constituents ($X_i^{t_q}, i = 1, 2, 3$):

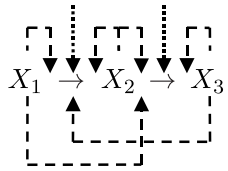

(7)

where the solid arrows ($\rightarrow$) denote the chemical transformations of the constituents, the broken-line arrows ($\dashrightarrow$) denote "information exchange" between the constituents inside each cell of the lattice, and the finely dotted arrows ($\cdots\!\blacktriangleright$) denote "information exchange" between the constituents in a particular cell and the constituents in the closest neighboring cells. For this particular mechanism, the following set of difference equations may be derived from CRDCD basic equations, with some assumptions regarding the model's parameters[9] ($q = 0, 1, 2, \ldots, Q$):

$$X_1^{t_q}(R_p, R_s) = \frac{b}{1 + \pi_1(X_i^{t_{q-1}}(r\otimes)) + \pi_1(X_i^{t_{q-1}}(r\otimes))\pi_2(X_i^{t_{q-1}}(r\otimes))} \tag{8}$$

$$X_2^{t_q}(R_p, R_s) = \frac{b\pi_1(X_i^{t_{q-1}}(r\otimes))}{1 + \pi_1(X_i^{t_{q-1}}(r\otimes)) + \pi_1(X_i^{t_{q-1}}(r\otimes))\pi_2(X_i^{t_{q-1}}(r\otimes))} \tag{9}$$

$$X_3^{t_q}(R_p, R_s) = \frac{b\pi_1(X_i^{t_{q-1}}(r\otimes))\pi_2(X_i^{t_{q-1}}(r\otimes))}{1 + \pi_1(X_i^{t_{q-1}}(r\otimes)) + \pi_1(X_i^{t_{q-1}}(r\otimes))\pi_2(X_i^{t_{q-1}}(r\otimes))} \tag{10}$$

$$\pi_1(X_i^{t_{q-1}}(r\otimes)) = k_1 \exp\left\{-\left[\sum_{i=1}^{3} \alpha_i X_i^{t_{q-1}}(R_p, R_s) + \sum_{i=1}^{3} \beta_i X_i^{t_{q-1}}(r\otimes)\right]\right\} \tag{11}$$

$$\pi_2(X_i^{t_{q-1}}(r\otimes)) = k_2 \exp\left\{-\left[\sum_{i=1}^{3} \alpha_i X_i^{t_{q-1}}(R_p, R_s) + \sum_{i=1}^{3} \beta_i X_i^{t_{q-1}}(r\otimes)\right]\right\}. \tag{12}$$

The mathematical model (8)–(10) presented above has nine parameters ($b, k_1, k_2, \alpha_1, \alpha_2, \alpha_3, \beta_1, \beta_2, \beta_3$) that should be defined according to the desired type of image (symmetrical, nonsymmetrical, spiral, etc.). For any given set of parameters of the model, Eqs. (8)–(10) generate a sequence of lattice-distributed concentrations of three chemical constituents $[X_1^{t_q}(R_p, R_s), X_2^{t_q}(R_p, R_s)$ and $X_3^{t_q}(R_p, R_s)]$. The calculations start from the initial conditions at t_0 [Eq. (5)] and continue up to t_Q (for any given Q). For each t_q, these solutions are mathematically represented by three 2D arrays of size $R \times R$: each array contains the calculated values of the concentrations $[X_1^{t_q}(R_p, R_s)$, $X_2^{t_q}(R_p, R_s)$ or $X_3^{t_q}(R_p, R_s)$, $R_p, R_s = 1, 2, \ldots, R]$. Therefore, the spatial-temporal dynamics of this system are defined by three sequences ($i = 1, 2, 3$) of 2D arrays, with the number of arrays in each sequence being the same as the number of iterations (Q). The following array comprises an example of the calculated concentrations of $X_1^{t_q}(R_p, R_s)$, presented here with the accuracy 10^{-2} ($R_p, R_s = 10$, $q = 100$, parameters $b = 0.09$, $k_1 = 10.98$, $k_2 = 3.99$, $\alpha_1 = -3.39$, $\alpha_2 = -5.18$, $\alpha_3 = -4.03$, $\beta_1 = 3.21$, $\beta_2 = -6.78$, $\beta_3 = 10.00$):

$$X_1^{t_{100}}(R_p, R_s) = \begin{pmatrix} 0 & 0.02 & 0.04 & 0.06 & 0.07 & 0.07 & 0.06 & 0.04 & 0.02 & 0 \\ 0.02 & 0.06 & 0.08 & 0.09 & 0.09 & 0.09 & 0.09 & 0.08 & 0.06 & 0.02 \\ 0.04 & 0.08 & 0.08 & 0.08 & 0.07 & 0.07 & 0.08 & 0.08 & 0.08 & 0.04 \\ 0.06 & 0.09 & 0.08 & 0.05 & 0.02 & 0.02 & 0.05 & 0.08 & 0.09 & 0.06 \\ 0.07 & 0.09 & 0.07 & 0.02 & 0 & 0 & 0.02 & 0.07 & 0.09 & 0.07 \\ 0.07 & 0.09 & 0.07 & 0.02 & 0 & 0 & 0.02 & 0.07 & 0.09 & 0.07 \\ 0.06 & 0.09 & 0.08 & 0.05 & 0.02 & 0.02 & 0.05 & 0.08 & 0.09 & 0.06 \\ 0.04 & 0.08 & 0.08 & 0.08 & 0.07 & 0.07 & 0.08 & 0.08 & 0.08 & 0.04 \\ 0.02 & 0.06 & 0.08 & 0.09 & 0.09 & 0.09 & 0.09 & 0.08 & 0.06 & 0.02 \\ 0 & 0.02 & 0.04 & 0.06 & 0.07 & 0.07 & 0.06 & 0.04 & 0.02 & 0 \end{pmatrix}.$$

In accordance with Eqs. (8)–(10), the values of the constituents' concentrations vary in the interval $0 < X_i^{t_q}(R_p, R_s) < b$. This interval may be encoded into colors by using a particular palette of C colors and therefore providing a resolution of b/C. On the basis of this scheme, each 2D array may be represented as a 2D colored image in the following manner: to each value in the array $[X_i^{t_q}(R_p, R_s)]$, a corresponding color from the palette is first assigned and then visualized as a pixel on the computer screen [the position of the pixel is specified by the coordinates (R_p, R_s). In this way, at each moment of discrete time, three images (for each of the three constituents) are generated.

3. RESULTS

One of the most important factors in the process of visualization of CRDCD arrays is the choice of the palette, i.e. the number of colors in the palette and their sequence (order). The fact that the calculated concentration values are continuous real numbers facilitates utilization of palettes with a practically unlimited number of colors [from two colors (black and white) up to the highest possible computer color quality (2^{32} on a standard PC)], which can be arranged in any order. By applying different palettes, we expect to observe patterns (existing on different numerical scales) that would possibly be invisible if the appropriate palette had not been chosen. Therefore, the number of colors in the palette (resolution) and the order of the colors in the palette play a role of "mathematical microscope" that can reveal additional embedded structural details when the appropriate palette is applied. To illustrate this idea, we used four different color palettes: a PC "true color" palette consisting of 2^{24} colors; a "random true color" palette consisting of the same 2^{24} PC colors arranged in arbitrary order; a "spectrum 256" palette consisting of 256 colors composed by the authors (Fig. 1a), and a "random 256" palette containing the same 256 colors arranged in arbitrary order (Fig. 1b).

In Fig. 2 (example 1), we present four symmetrical images visualized with the four above-described color palettes. It can be seen that different patterns were obtained for the same "source" 2D array calculated by Eqs. (7)–(10) $[X_1^{t_q}(R_p, R_s)$, 100×100, $q = 150$, parameters: $b = 0.0936$, $k_1 = 10.9754$, $k_2 = 3.9944$, $\alpha_1 = -3.3872$, $\alpha_2 = -5.1812$, $\alpha_3 = -4.0286$, $\beta_1 = 3.2097$, $\beta_2 = -6.7845$, $\beta_3 = 10.0000]$. Owing to the continuous nature of the concentration values $[0 < X_i^{t_q}(R_p, R_s) < b]$ calculated with computer accuracy (10^{-16}), the visualization by $\sim 16 \times 10^6$ colors ("true color" and "true random color") resulted in a display of

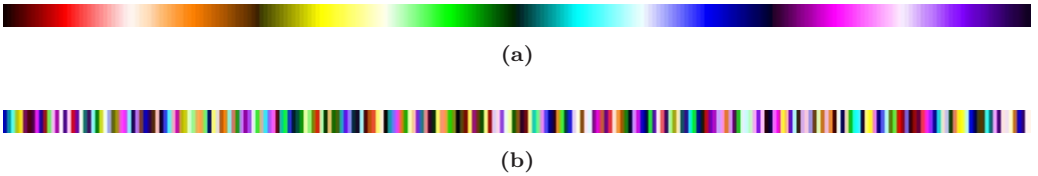

(a) **(b)**

Fig. 1 Two color palettes of 256 colors: (**a**) "spectrum 256" palette; and (**b**) "random 256" palette.

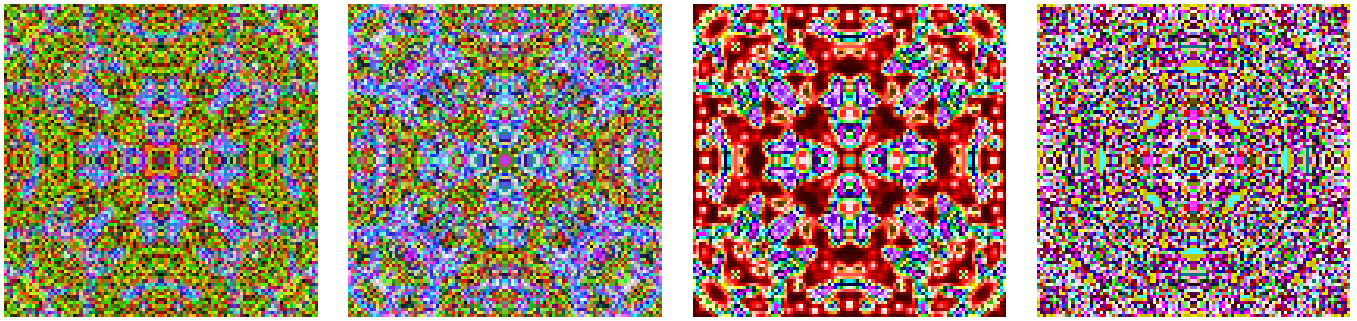

(a) **(b)** **(c)** **(d)**

Fig. 2 Example 1. Visualization of a 2D array $X_1^{t_q}(R_p, R_s)$ (100×100 pixels, $q = 150$) with four different palettes: **(a)** "true color," **(b)** "random true color," **(c)** "spectrum 256," and **(d)** "random 256."

the concentration values having the finest distinctions in color (Figs. 2a and 2b). The other two images (Figs. 2c and 2d) were created using less fine visualization (256 colors), and due to the difference in the order of the colors, differences in the internal patterns could be seen. Visualization with the "spectrum 256" palette revealed distinct well-colored patterns (Fig. 2c), while the image created with the "random 256" palette was variegated, with the internal patterns hardly being visible (Fig. 2d).

Another example of the application of four different palettes [for the "source" array $X_1^{t_q}(R_p, R_s)$, 100×100, $q = 150$, parameters: $b = 0.1048$, $k_1 = 0.5158$, $k_2 = 0.0001$, $\alpha_1 = -10$, $\alpha_2 = -9.2763$, $\alpha_3 = -10$, $\beta_1 = -0.4229$, $\beta_2 = -10$, $\beta_3 = 3.3222$] is presented in Fig. 3 (example 2). This example shows that both "true color" palettes revealed the patterns in the central part of the "source" array that were not visible with the 256 color palettes.

From the examples presented above, we can conclude that from an aesthetic point of view no particular palette can be considered optimal for visualization of CRDCD arrays, but for mathematical imaging of real physicochemical patterns, the choice of the palette should be conditional upon the accuracy of the experimentally obtained data [$X_1^{t_q}(R_p, R_s)$ experimental]. If so, the choice of a particular palette will be related to the experimentally verified patterns, or their parts, and the mathematical imaging based on the proposed CRDCD model will serve for data interpolation and extrapolation. Therefore, the palette should be considered as an additional parameter of the CRDCD model, which should be defined by analysis of the experimental data in the same way that the other parameters of the model are defined.[9]

Another factor that affects the resulting CRDCD image is the size R of the lattice. In Fig. 4, we present three examples of images calculated and visualized with the same parameters, except for the lattice size, which is set at 50×50 pixels (Fig. 4a), 150×150 pixels (Fig. 4b) or 200×200 pixels (Fig. 4c). As can be seen, the greater the lattice size, the more complicated the internal patterns that appear on the image. However, preservation of some basic patterns can be observed. Therefore, the size of the lattice R also should be used as an independent parameter of the model, which affects the resulting images, and should be verified experimentally.

To improve the quality of the CRDCD image and to conserve the desired "source patterns" on the enlarged image, interpolation should be applied. Images generated with CRDCD allow interpolation to be applied directly using concentration values (2D arrays). To reach the desired "smoothing" within the generated pattern, we used the following scheme. First, the chosen number G of "interpolating" cells ($g = 1, 2, 3, \ldots, G$) was inserted between each pair of neighboring cells in the "original" lattice in both the vertical direction [between $X_1^{t_q}(R_p, R_s)^{\text{orig}}$ and $X_1^{t_q}(R_{p+1}, R_s)^{\text{orig}}$] and the horizontal direction [between $X_1^{t_q}(R_p, R_s)^{\text{orig}}$ and $X_1^{t_q}(R_p, R_{s+1})^{\text{orig}}$]. Then, the interpolation formula was applied, and the new concentration values $X_1^{t_q}(R_p, R_s)_g^{\text{inter}}$ within the inserted (interpolating) cells were calculated. The following results were obtained for the linear

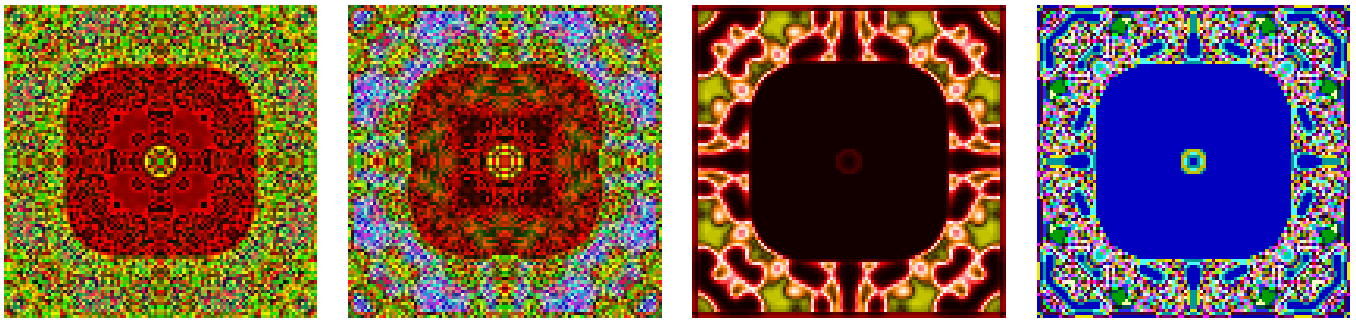

(a) **(b)** **(c)** **(d)**

Fig. 3 Example 2. Visualization of a 2D array $X_1^{t_q}(R_p, R_s)$ (100×100 pixels, $q = 150$) with four different palettes: **(a)** "true color," **(b)** "random true color," **(c)** "spectrum 256," and **(d)** "random 256."

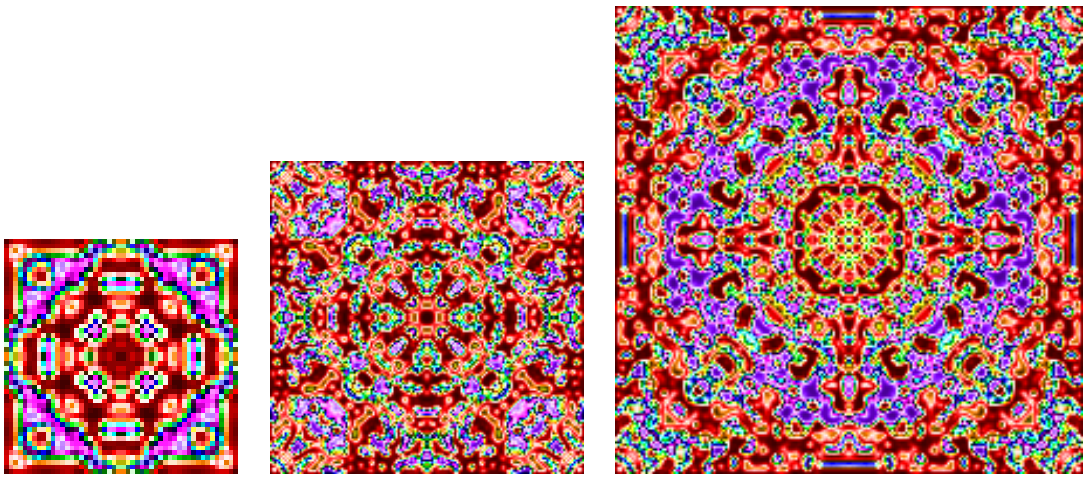

(a) **(b)** **(c)**

Fig. 4 Example of three images $X_1^{t_q}(R_p, R_s)$ ($q = 250$) visualized with a "spectrum 256" palette and calculated for different lattice sizes: **(a)** 50×50 pixels, **(b)** 150×150 pixels and **(c)** 200×200 pixels.

interpolation:

$$X_1^{t_q}(R_p, R_s)_g^{\text{inter}} = \begin{cases} X_1^{t_q}(R_p, R_s)^{\text{orig}} \\ \quad + g\left(\dfrac{X_1^{t_q}(R_{p+1}, R_s)^{\text{orig}} - X_1^{t_q}(R_p, R_s)^{\text{orig}}}{G+1}\right), \\ \qquad\qquad \text{vertical} \\ X_1^{t_q}(R_p, R_s)^{\text{orig}} \\ \quad + g\left(\dfrac{X_1^{t_q}(R_p, R_{s+1})^{\text{orig}} - X_1^{t_q}(R_p, R_s)^{\text{orig}}}{G+1}\right), \\ \qquad\qquad \text{horizontal.} \end{cases} \tag{13}$$

In this way, a qualitative smooth image of any size can be obtained. In Fig. 5b we present the interpolated image (three inserted cells, 397×397 pixels) obtained for the 2D array source that is shown in Fig. 5a ($X_1^{t_q}(R_p, R_s)$, 100×100, $q = 150$). The visualization of both the interpolated and source arrays was performed with the "spectrum 256" palette. As can be seen, all the internal patterns existing in the source image were preserved, but the quality of the visual representation was improved by interpolation.

CRDCD difference equations produce sequences of images that simulate space-distributed chemical reaction dynamics of the chemical system's constituents. To enable the investigator to observe

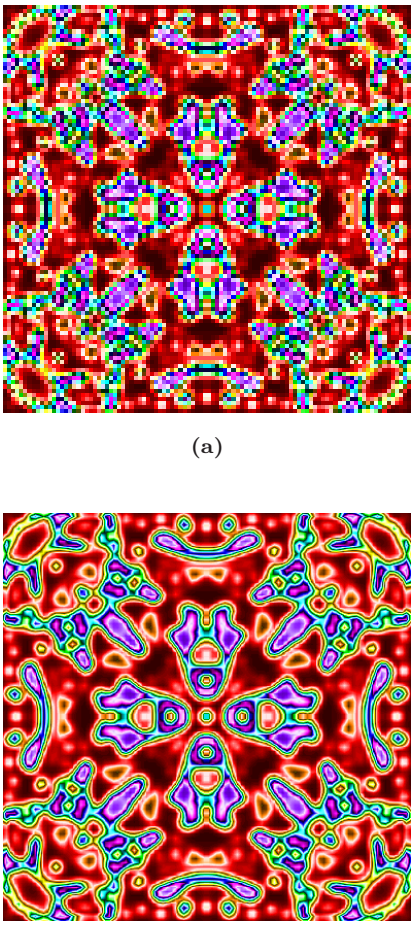

(a)

(b)

Fig. 5 **(a)** Image without interpolation, corresponding to the "source" array $X_1^{t_q}(R_p, R_s)$ (100×100, $q = 150$) and **(b)** image interpolated according to Eq. (13).

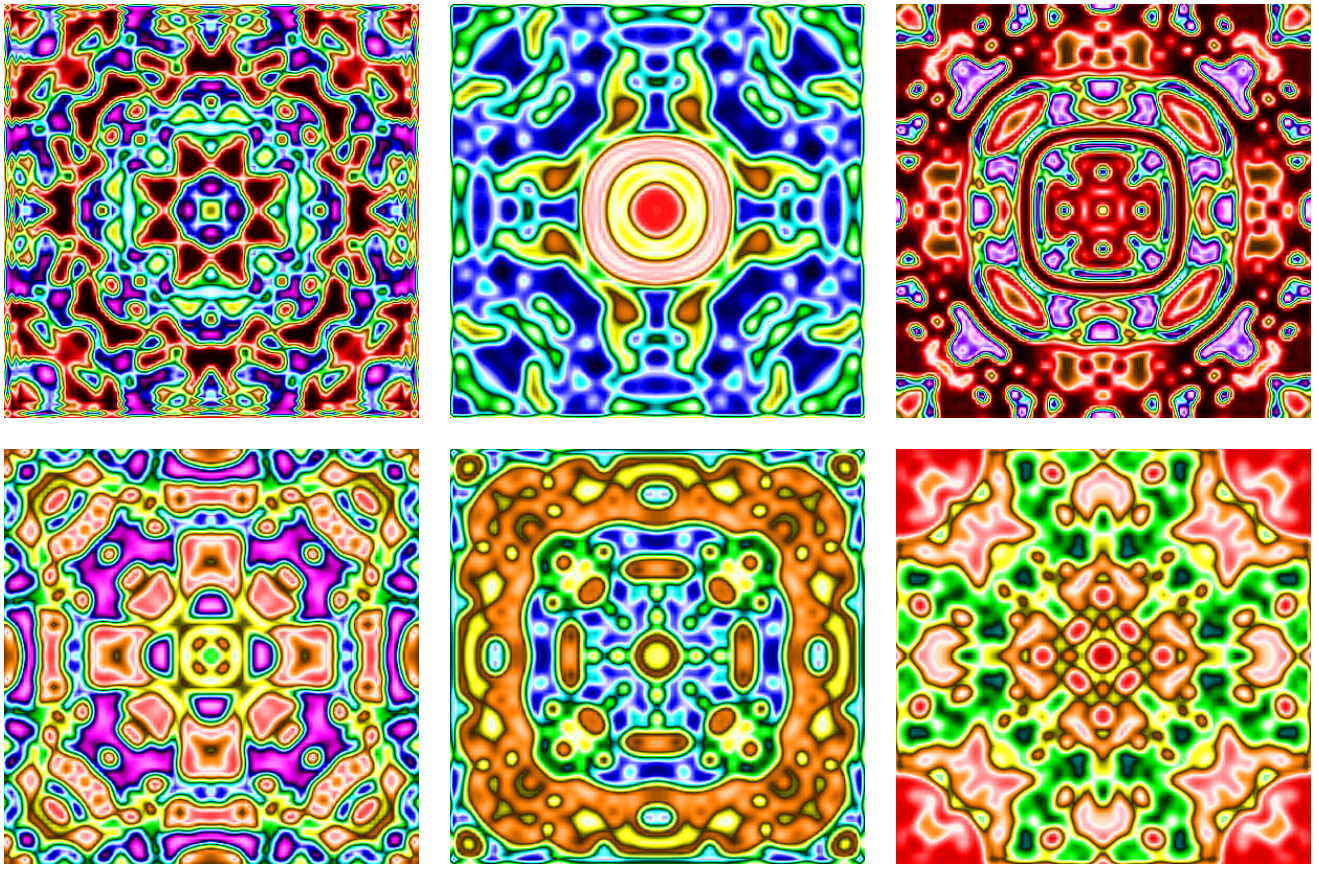

Fig. 6 Examples of images generated by varying the parameters of the model and visualized with the "spectrum 256" palette after interpolation.

the evolution of a constituent in real time, we need to correlate the particular sequence of images calculated by CRDCD, which appear at the rate of computer calculations, with the time of the physicochemical experiments. For this purpose, a different scheme of animation could be applied and the desired effect — visual dynamic perception of the evolution of the processes — could be achieved. For example, sequences of symmetrical images generated by CRDCD equations produce a kaleidoscope effect when a sequence of Q images appears periodically, with the proper time interval having been chosen between the images. An additional animation effect can be achieved by applying interpolation: in this case, we insert a number of intermediate images, produced by interpolation between two "original" images generated by CRDCD. This method facilitates the transformation of the kaleidoscope effect into smooth animation, in which the images "spill over," one into another.

Some additional examples of symmetrical images calculated with different sets of parameters of the model parameters are presented in Fig. 6. These images comprise the visualization of interpolated "original" 2D arrays of size 100×100 with the "spectrum 256" palette.

4. CONCLUSIONS

By using a concrete example [Eqs. (8)–(10)] derived from basic CRDCD equations [Eqs. (2)–(4)], we have shown that the patterns inherent in CRDCD mathematical models can be visualized. Because of the continuous character of the concentrations of a reaction's constituents, CRDCD-based mathematical imaging facilitates the application of colored palettes with an arbitrary number of colors for visualization of calculated 2D arrays. By changing the parameters of the equations, the type of palette and the size of the lattice, a variety of different symmetrical images can be obtained. Nonsymmetrical images of different patterns can also be generated by CRDCD, as previously described in Gontar.[7] We are therefore confident that there

are practical applications for the described method for mathematical modeling and visualization of the dynamics of complex physicochemical systems, such as the system of interconnected neurons (simulation of brain creativity in a form of artistic patterns),[8] colonies of living cells and the evolution of microbes (processes of self-organization), multiagent subatomic systems, image processing, computer graphics, artistic image design and animation.

REFERENCES

1. B. B. Mandelbrot, *Fractals and Chaos* (Springer, New York, 2004).
2. H. Peitgen, H. Jurgens and D. Saupe, *Chaos and Fractals* (Springer-Verlag, 2004).
3. S. Wolfram, *A New Kind of Science* (Wolfram Media, 2002).
4. P. Prusinkiewicz and J. Hanan, Lindenmayer systems, fractals, and plants, in *Lecture Notes in Biomathematics*, Vol. 79 (Springer-Verlag, 1989).
5. M. A. Nowak and R. M. May, The spatial dilemmas of evolution, *Int. J. Bifurcat. Chaos* **3** (1993) 35–78.
6. V. Gontar and A. V. Il'in, New dynamical model describing spatio-temporal behavior of chemical reactions, *Physica D* **52** (1991) 528–531.
7. V. Gontar, Theoretical foundation for the discrete chaotic dynamics of physicochemical systems: chaos, self-organization, time and space in complex systems, *Discr. Dyn. Nat. Soc.* **1**(1) (1997) 31–44.
8. V. Gontar, Artificial brain systems based on discrete chaotic dynamics of interacting intellectual agents, in *Proc. Int. Conf. Comput. Sci. Its Appl.* (National University, San-Diego, USA, 2003).
9. V. Gontar and O. Grechko, Generation of symmetrical colored images via solution of the inverse problem of chemical reactions discrete chaotic dynamics, *Int. J. Bifurcat. Chaos* **16**(5) (2006) 1419–1434.